# Traveltime computation by wavefront-oriented ray-tracing

*R. Coman and D. Gajewski*

**email:** *coman@dkrz.de*

**keywords:** *traveltimes, ray tracing, accuracy*

**ABSTRACT**

*For multivalued traveltime computation, we propose a wavefront-oriented ray-tracing technique. At the source, we start with few rays which are propagated stepwise through a smooth two-dimensional (2D) velocity model. The ray field is examined at wavefronts and a new ray is inserted between two adjacent rays if one of the following criteria is satisfied: (1) the distance between the adjacent rays is larger than a predefined threshold, (2) the difference in wavefront curvature between the adjacent rays is larger than a predefined threshold, (3) the adjacent rays cross each other. We insert the new ray by tracing it from the source. This is a more accurate approach than the insertion of a new ray by interpolation on the wavefront. The traveltimes computed along the rays are used for the estimation of traveltimes on a rectangular grid. This estimation is carried out within a region bounded by adjacent wavefronts and rays. Considering the wavefront curvature, we extrapolate the traveltimes from the intersection points between rays and wavefronts to the gridpoint. The extrapolated values are weighted with respect to the distances to wavefronts and rays. Because dynamic ray tracing is not applied, we approximate the wavefront curvature at a given point using the slowness vector at this point and an adjacent point on the same wavefront. We analyze the influence of the input parameters which control the wavefront and ray densities on the accuracy and the computational speed of the proposed technique. We relate the wavefront and ray densities to the shortest spatial wavelength of the smooth velocity model and show that the proposed wavefront-oriented ray-tracing technique permits an accurate traveltime computation using a small number of rays and wavefronts.*

## INTRODUCTION

During the last years several papers have shown the importance of multivalued traveltime tables for the quality of migrated images (Geoltrain and Brac, 1993; Ettrich and Gajewski, 1996; Operto et al., 2000). However, multivalued traveltime tables are not widely used because their computation is time consuming. In this paper we present a method for an efficient computation of multivalued traveltime tables in smooth two-dimensional velocity models.

Multivalued traveltime tables are usually computed by ray methods which propagate a ray field rather than a single ray. To increase the efficiency of these methods, adjacent rays are grouped into ray tubes, the ray density of the ray field is checked at certain positions, and if necessary, new rays are inserted. The ray field may be examined at constant depth levels (Lambaré et al., 1992), at interfaces (Åstebøl, 1994), at the final surface (Bulant, 1999), or at the wavefronts. The last approach was introduced by Vinje et al. (1993) and appears to be the most powerful one. Since then, several improvements and other related implementations of the method have been proposed (Sun, 1992; Vinje et al., 1996a,b; Lambaré et al., 1996; Ettrich and Gajewski, 1996; Lucio et al., 1996; Moser and Pajchel, 1997; Vinje, 1997; Bulant and Klimeš, 1999). Methods which check the ray field at wavefronts, are called wavefront construction (WFC) methods.

The main characteristics of the WFC methods are (see also Figure 1) :

- The propagation of the ray field with a constant traveltime step (wavefront propagation).
- The insertion of a new ray between two adjacent rays. Usually, a new ray is inserted by interpolation on the wavefront. The technique which we propose – the wavefront-oriented ray-tracing (WRT) technique – inserts a new ray by tracing it from the source. We also introduce new criteria for the insertion of new rays.
- The estimation of ray quantities (e.g., traveltimes) within a ray cell, which is the part of the ray tube between the last two constructed wavefronts. The ray quantities are estimated (usually by interpolation) from the intersection points between wavefronts and rays onto a rectangular grid. We estimate the traveltime at the gridpoints by a distance-weighted average of extrapolated traveltimes.

In the following we use the term *cell* instead of ray cell and *node* as a shortcut for the intersection point between wavefronts and rays (see Figure 1).

The insertion of a new ray by interpolation on the wavefront is considered to be a key feature of the WFC methods (e.g., Vinje et al., 1993). However, we prefer to insert a new ray by tracing it from the source because of the higher accuracy. This insertion approach also permits a lower ray density. The insertion of a new ray by tracing it from the source was also used in the controlled initial-value ray-tracing algorithm by Bulant, (1999). In this algorithm, the wave field is estimated only at the final surface and the decomposition into cells is completely separated from the interpolation of traveltimes. Checking the ray field only at the final surface, however, leads to oversampling by cells and the advantages of the WFC methods are only partly used. The WRT technique generates only a small number of cells, because it starts with few rays and inserts a new ray only when necessary.

Usually, two main classes of criteria have been used to decide whether to insert a new ray. The first class (e.g., Sun, 1992) uses the distance between two adjacent nodes and the difference in direction between adjacent rays, while the second class (e.g., Lambaré et al., 1996) uses the error of the paraxial approximation in terms of coordinates and slownesses. The first class of criteria leads to undersampling in caustic regions (Lambaré et al., 1996), while the second one might overlook small-scale velocity anomalies. None of the above mentioned criteria are directly

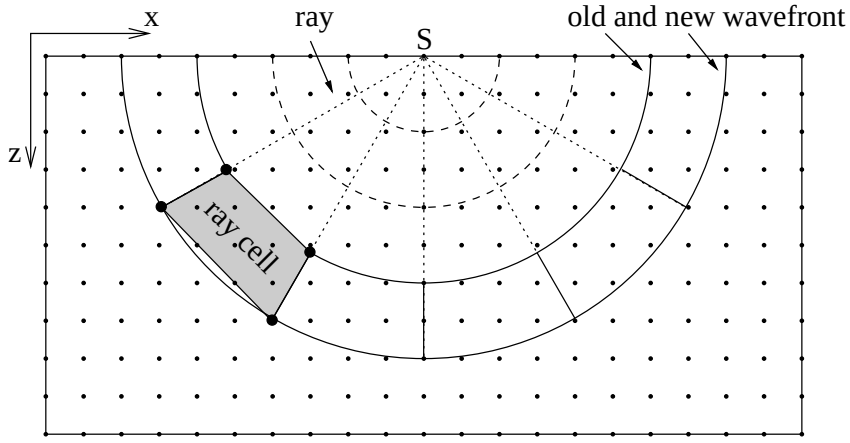


**Figure 1:** Graphical description of the WFC methods. The traveltimes at nodes (large dots) are computed by ray tracing. The traveltimes at gridpoints (small dots) are estimated within a ray cell. Point $S$ denotes the source point.

connected with the traveltime errors. To control this errors, Vinje (1997) suggested an insertion criterion based on probe rays. This criterion is limited to relative traveltime errors and does not consider the traveltime errors generated by a wrong direction of the interpolated ray.

We insert a new ray if one of the following criteria is satisfied: (1) the distance between the adjacent rays is larger than a predefined threshold, (2) the difference in wavefront curvature between the adjacent rays is larger than a predefined threshold, (3) the adjacent rays cross each other. The criterion based on the distance between nodes avoids overlooking of small-scale velocity anomalies, while the criterion based on the wavefront curvatures controls the error of the traveltime estimation within the cells. The third criterion increase the ray density in caustic zones. These criteria allow to control the accuracy of the WRT technique.

For the estimation of ray quantities (e.g., traveltimes, slownesses, amplitudes) within cells, Vinje et al. (1993) projected the gridpoint on the old wavefront (for old wavefront see Figure 1), interpolated the ray quantities at the projection point and traced a ray back to the gridpoint. Lambaré et al. (1996) split the cell into two triangles and performed linear interpolation within triangles, while Bulant and Klimeš (1999) proposed a bicubic interpolation of traveltimes. Here, we propose a distance-weighted average of extrapolated traveltimes. The extrapolation is performed from nodes to gridpoints under consideration of the wavefront curvature.

The WRT technique uses a grid-based smooth velocity model. The velocity and its first derivatives are estimated at an arbitrary point by bilinear interpolation. A similar model representation has been used by Ettrich and Gajewski (1996).

The efficiency of the WRT technique strongly depends on the input parameters which control the wavefront and ray densities. On the basis of traveltimes computed in a smoothed Marmousi model, we analyze these dependencies and suggest some rules for a correct choice of input parameters.

## DESCRIPTION OF THE METHOD

### Propagation of wavefronts

The propagation of the ray field is done by kinematic ray tracing (KRT). For the 2D case, the KRT system is given by (e.g., Červený, 1985)

$$\frac{dx_I}{d\tau} = v^2 p_I, \tag{1}$$

$$\frac{dp_I}{d\tau} = -\frac{1}{v}\frac{\partial v}{\partial x_I}, \quad I = 1, 2 \tag{2}$$

where $x_1$ and $x_2$ are the horizontal and vertical Cartesian coordinates; $p_1$ and $p_2$ are the components of the slowness vector; $v$ is the velocity, $\tau$ the traveltime. To solve the KRT system we use a fourth-order Runge-Kutta method. We call the integration step of the Runge-Kutta method *time step of rays*. A new wavefront is constructed from the old one by propagating the ray field with a constant traveltime step (*time step of wavefronts*). The time step of wavefronts can be the same as the time step of rays, the time step of wavefronts can be a multiple of the time step of rays.

After the construction of a new wavefront, we estimate the traveltimes in the region between this wavefront and the previous one. Therefore, only two wavefronts are simultaneously stored in the computer memory. For each node on these wavefronts, we store the Cartesian coordinates, the slowness components of the ray, and the take-off angle of the ray.

Usually, the rays which are used for the propagation of the wavefront do not pass the gridpoints. To estimate the traveltimes at gridpoints, we approximate the wavefront between two adjacent rays, and consider the wavefront curvature for the extrapolation of the traveltimes from nodes to gridpoints. The approximation of the wavefront curvature is described in the next section.

### Approximation of the wavefront curvature

The standard way to compute the wavefront curvature is dynamic ray tracing (e.g., Červený, 1985). Because the WRT technique does not apply dynamic ray tracing, we approximate the wavefront curvature at a given node using the slowness vector at this node and an adjacent node on the same wavefront. These position of the nodes and the direction of the slowness vector are sufficient to construct a circle which passes the nodes. We approximate the radius of the wavefront curvature at the given point by the radius of this circle (Figure 2).

The wavefront curvature is used not only for the extrapolation of traveltimes within cells but also as an insertion criterion for new rays. The insertion approach is described in the next section.

### Insertion of new rays

In this section, we present the approach used for the insertion of a new ray and the criteria used for the decision when to insert a new ray. Our goal is to compute accurate traveltimes using a minimal number of rays (optimal ray density).

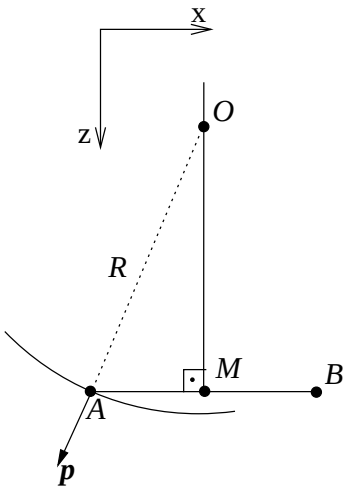


**Figure 2:** Approximation of the wavefront curvature. The radius R of the wavefront curvature at node $A$ is approximated by the distance $|\overline{OA}|$. Point $M$ is the midpoint of the segment $\overline{AB}$. Point $O$, which is obtained by the intersection of the continuation of the slowness vector $\mathbf{p}$ at $A$ with the normal to the segment $\overline{AB}$ at $M$, is the center of the circle which passes the nodes $A$ and $B$.

Usually, a new ray is inserted by interpolation between two adjacent rays (parent rays) on the wavefront. Because of higher accuracy, we prefer to insert a new ray by tracing it from the source. The ray quantities of the traced ray have the same accuracy as the ray quantities of the parent rays, while the accuracy of the interpolated rays is always worser than the accuracy of the parent rays. Moreover, the accuracy of the ray inserted by tracing does not depend on the distance between the parent rays. In conclusion, the insertion of a new ray by tracing is not only more accurate but also permits a lower ray density than the insertion by interpolation. The initial direction of the traced ray is given by the bisector of the angle between the parent rays at the source.

We insert a new ray if one of the following criteria is satisfied: (1) the distance between two adjacent nodes exceeds a predefined threshold (node-distance threshold), (2) the difference in wavefront curvature between two adjacent rays exceeds a predefined threshold (time-difference threshold, see below), (3) two adjacent rays cross each other.

Note that we prefer to express the difference in wavefront curvature in time units (milliseconds). For this reason we divide the difference of the radii of curvature by the velocity at the midpoint between the adjacent nodes. In the following we use *time difference* as a shortcut for the difference in wavefront curvature between two adjacent rays and *node distance* for the distance between two adjacent nodes.

There are regions where rays cannot be sent directly form the source (shadow zones). If the distance between adjacent rays exceeds twice the node-distance threshold, we allow new rays to be inserted by interpolation on the wavefront. For details about this insertion procedure see Ettrich and Gajewski (1996).

An optimal ray density is a precondition for an accurate estimation of traveltimes within cells.

This estimation is described in the next section.

### Estimation of traveltimes within ray cells

Using KRT, the traveltimes are computed along the rays at nodes, but for Kirchhoff depth migration the traveltimes are needed on a rectangular grid. The WRT technique uses the node-traveltimes to estimate the gridpoint-traveltimes.

The estimation is carried out within cells, which are usually quadrangular. Non-quadrangular cells are used close to the boundary of the model. The quadrangular cells are delimited by two adjacent ray segments and two adjacent wavefront segments (Figure 3). Ray segments and wavefront segments are the linear local approximation of rays and wavefronts. The corners of quadrangular cells usually correspond to nodes, but a special situation occurs when a new ray is inserted. In order to ensure that the new cells are in contact with the preceding cell, the node of the inserted ray is projected onto the wavefront segment of the preceding cell (Figure 3). A similar approach was used by Lucio et al. (1996).

For an accurate estimation, the gridpoint has to be within the cell. To satisfy this requirement, we bound the cell by a rectangular area and check each gridpoint in this area for its position relative to the cell. To decide if the gridpoint is inside or outside the cell, we use the approach proposed by Ettrich and Gajewski (1996).

We have mentioned above that the insertion of a new ray by tracing from the source permits a low ray density corresponding to large cell. Because linear interpolation in large cells is not sufficient, we propose a distance-weighted averaging of extrapolated traveltimes instead. The traveltimes are extrapolated from nodes to a gridpoint considering the wavefront curvature at the nodes. The extrapolated values are weighted with respect to the distances from the gridpoint to the ray-segments and to the wavefront-segments.

## NUMERICAL EXAMPLES

The aim of the following numerical examples is to show the influence of the input parameters (time step of wavefronts, node-distance threshold, time-difference threshold) on the accuracy and the computational speed of the WRT technique. The results allow to propose some rules for the choice of suitable input parameters. The numerical tests are carried out in a smoothed version of the Marmousi model (Versteeg and Grau, 1990), where structures of spatial dimension lower than 200 m are removed (Figure 4a,b). The velocity grid has been resampled from 4 m to 20 m after smoothing.

We compute the traveltimes for five sets of input parameters, which are given in Table 1. The first set of input parameters is tuned in order to compute reference traveltimes (it is not possible to compute analytical traveltimes for complex models) and to estimate the number of later-arrival traveltimes. To analyze the influence of the input parameters on the computational speed, we consider the results from the second parameter set as a reference. For the last three numerical examples, we change only one input parameter and keep the other parameters as in the second set. To ensure that the traveltime errors are not related to the ray-tracing procedure, we use the same time step of rays ($10$ ms) in all five examples (see Table 1). The source is located

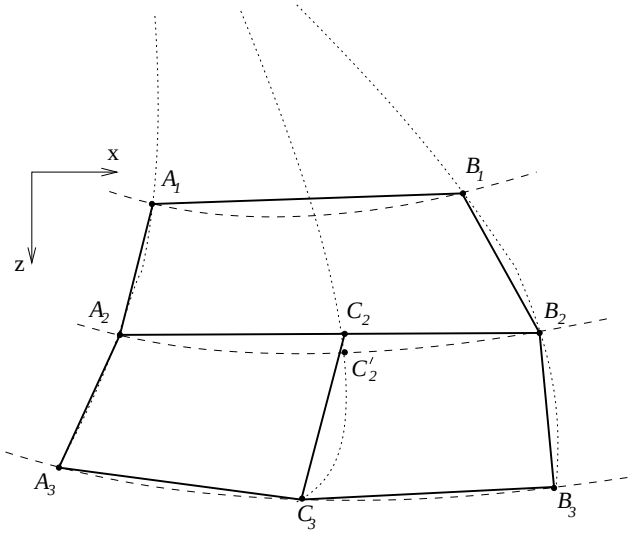


**Figure 3:** Rays, wavefronts and cells. The dotted lines are rays, the dashed lines are wavefronts, and the solid lines are linear ray or wavefront segments. The dotted line $C_2'C_3$ is a newly inserted ray. The quadrangles indicated by solid lines are cells. In most cases the cell corners lie on nodes. Exceptions occur when a new ray is inserted. To ensure a continuous coverage with cells the node $C_2'$ is projected on the wavefront segment $A_2B_2$ ($C_2'C_2$ is perpendicular to the solid line $A_2B_2$).

at coordinates $x = 6$ km and $z = 0$ km.

The accuracy of the proposed method depends on the accuracy of the ray-tracing procedure, the accuracy of the insertion of new rays, and the accuracy of the estimation of traveltimes within cells. Using the fourth-order Runge-Kutta method, the accuracy of the ray-tracing procedure can be increased by decreasing the time step of rays. The errors connected with the insertion of a new ray are the same as the errors of the ray-tracing procedure because the new ray is traced directly from the source. Because a proper choice of the time step of rays permits a highly accurate propagation of rays, the absolute traveltime errors are mainly given by the errors introduced by the estimation of traveltimes within cells. The accuracy of this estimation can be increased by increasing the ray and wavefront densities.

We quantify the accuracy of the estimated traveltimes with respect to the reference traveltime by the mean traveltime error (expressed in milliseconds) and the percentage of arrivals with a traveltime error larger than a predefined value (in this case 0.4 ms).

The total CPU-time mainly consists of the time required for the propagation of rays, the time for the approximation of the wavefront curvature at nodes, and the time for the estimation of ray quantities at gridpoints. The CPU-time needed for the propagation of rays depends on the number of rays, while the CPU-time needed for the approximation of the wavefront curvature depends on the number of cells. The CPU-time needed for the estimation of ray quantities depends on the density of the output grid. The traveltimes can be estimated on a fine grid, which can be directly used for Kirchhoff migration, or on a coarse grid. For practical applications, traveltimes are computed on a coarse grid and interpolation from the coarse grid to the fine grid is performed

during the migration process. For the interpolation from coarse grids to fine migration grids, we recommend the hyperbolic interpolation (Vanelle and Gajewski, 2001).

Since we use a fine output grid (grid distance 20 m) in our examples, most of the CPU-time is used for the estimation of traveltimes on this grid. We choose a fine grid because it permits a better graphical representation of the spatial distribution of the traveltime errors. For practical applications, however, the traveltimes are estimated on a coarser grid (which can have e.g., 100 times less gridpoints), and in this case the number of rays and cells is the most important factor for the computational speed. Therefore, we quantify the computational speed by the number of rays and cells. Actually, the number of cells is a more sensitive criterion because it includes the number of rays and it also depends on the number of wavefronts.

Beside the accuracy and the computational speed, we also analyze the influence of the insertion criteria on the number of later-arrivals found. This number depends on the ray density in caustic regions.

In the first numerical example (reference data for traveltimes and for the number of later-arrivals) we compute multivalued traveltime tables and estimate the number of later-arrivals by using a huge number of rays and cells (see Table 1). Because a lower time step of rays and a higher ray and wavefront density does not noticeable change the values of the traveltimes, we define the traveltimes computed with the parameter set 1 as reference traveltimes. A new ray is inserted if the node-distance becomes larger than 50 m, or if the time-difference becomes higher than 1 ms. Figure 4c shows isochrones, which are obtained from the reference traveltimes.

In the second example (reference data for the number of rays and cells), we set the time step of wavefronts to 40 ms, the time-difference threshold to 4 ms, and the node-distance threshold to 200 m. The resulting maximum number of rays is 318 and the number of cells is 2466. A number of 14850 later-arrivals are found (96 % of the number of later-arrivals which are computed in the first example). The decomposition of the model into cells is displayed in Figure 5a. Note the uniform distribution of first-arrival rays and the high ray density in the caustic regions. Most of the rays are inserted because the node-distance between adjacent rays becomes larger than 200 m. The spatial distribution of traveltime errors (Figure 5b) follows both rays and wavefronts. The mean traveltime error is 0.09 ms. Except for the boundary regions, there is only a small region at an offset of 7 km and a depth of 2.2 km with an error larger than 2 ms. More than 70 % of the errors are smaller than 0.1 ms and only 2.8 % are larger than 0.4 ms.

In the third example, we set the time step of wavefronts to 20 ms and keep the other input parameters as in the second example. As expected the number of cells gets larger, because the number of wavefronts is doubled. The decomposition of the model into cells is shown in Figure 6a. Because the distance between adjacent rays is larger than the distance between adjacent wavefronts, the spatial distribution of the errors follows the rays (Figure 6b). Compared to the second example, the accuracy of the computed traveltime increases (the mean error decreases from 0.09 ms to 0,06 ms) and the computational speed decreases (the number of rays and cells increase, see Table 1). Because the accuracy of the second example is sufficient for practical applications (more than 99 % of the traveltimes have errors smaller than 1 ms), a further increase of the accuracy does not justify the decrease of computational speed. The computational speed can be increased by using a larger time step of wavefronts (e.g., 80 ms), but the accuracy (which is comparable to the accuracy obtained for the fifth set of input parameters) might not be enough

| Example number | 1 | 2 | 3 | 4 | 5 |
|---|---|---|---|---|---|
| Time step of rays [ms] | 10 | 10 | 10 | 10 | 10 |
| Time step of wavefronts [ms] | 10 | 40 | 20 | 40 | 40 |
| Time-difference threshold [ms] | 1 | 4 | 4 | 8 | 4 |
| Node-distance threshold [m] | 50 | 200 | 200 | 200 | 400 |
| Max. number of rays | 150518 | 318 | 374 | 237 | 216 |
| Number of cells | 2334337 | 2466 | 5052 | 2206 | 1692 |
| Number of later-arrivals found | 15428 | 14850 | 14820 | 14143 | 13517 |
| Mean traveltime error [ms] | - | 0.09 | 0.06 | 0.10 | 0.39 |
| Arrivals with errors > 0.4 ms [%] | - | 2.8 | 1.3 | 2.9 | 26.2 |

**Table 1:** Five sets of input parameters and the resulting quantities used for the estimation of the efficiency of the WRT technique.

for practical applications.

In the fourth example, we set the time-difference threshold to 8 ms and keep the other input parameters as in the second example. The number of rays decreases by 22 %, and the number of cells by 10 %. At a first glance there is no difference between the distribution of cells in the second example and in the fourth example (Figure 5a and Figure 7a). Moreover, the spatial and percentual distribution of the traveltimes errors are nearly the same (Figure 5b and Figure 7b). However, a more careful comparison of the cell distribution shows differences in the caustic regions. As a consequence the number of later-arrivals which are found decreases by 5 % compared to the second example.

In the fifth example, we set the node-distance to 400 m and keep the other input parameter as in the second example. The number of rays decreases by 32 %, and the number of cells by 31 %. In contrast to the fourth example, this decrease of rays and cells is connected with a sizeable increase of the traveltime error. The mean traveltime error is four times larger than in the second example, and 26.2 % of arrivals have a traveltime error larger than 0.4 ms. The spatial distribution of the error follows the rays. This example shows the importance of the node-distance criterion for the accuracy of the computed traveltimes.

## CONCLUSIONS

For multivalued traveltime computation, we have presented the wavefront-oriented ray-tracing (WRT) technique. The technique starts with few rays which are propagated stepwise through a smooth two-dimensional (2D) velocity model. To retain an optimal ray density, we insert a new ray by tracing it from the source. This insertion approach is more accurate than the insertion of a new ray by interpolation on the wavefront and it permits a larger distance between adjacent rays. The traveltimes which are computed along the rays are used for the estimation of traveltimes on a regular grid. The estimation is carried out in a region delimited by ray and wavefront segments using a distance-weighted average of extrapolated traveltimes. The extrapolation is performed from nodes to gridpoints considering the wavefront curvature. Because we do not apply dynamic ray tracing, we approximate the wavefront curvature using quantities obtained

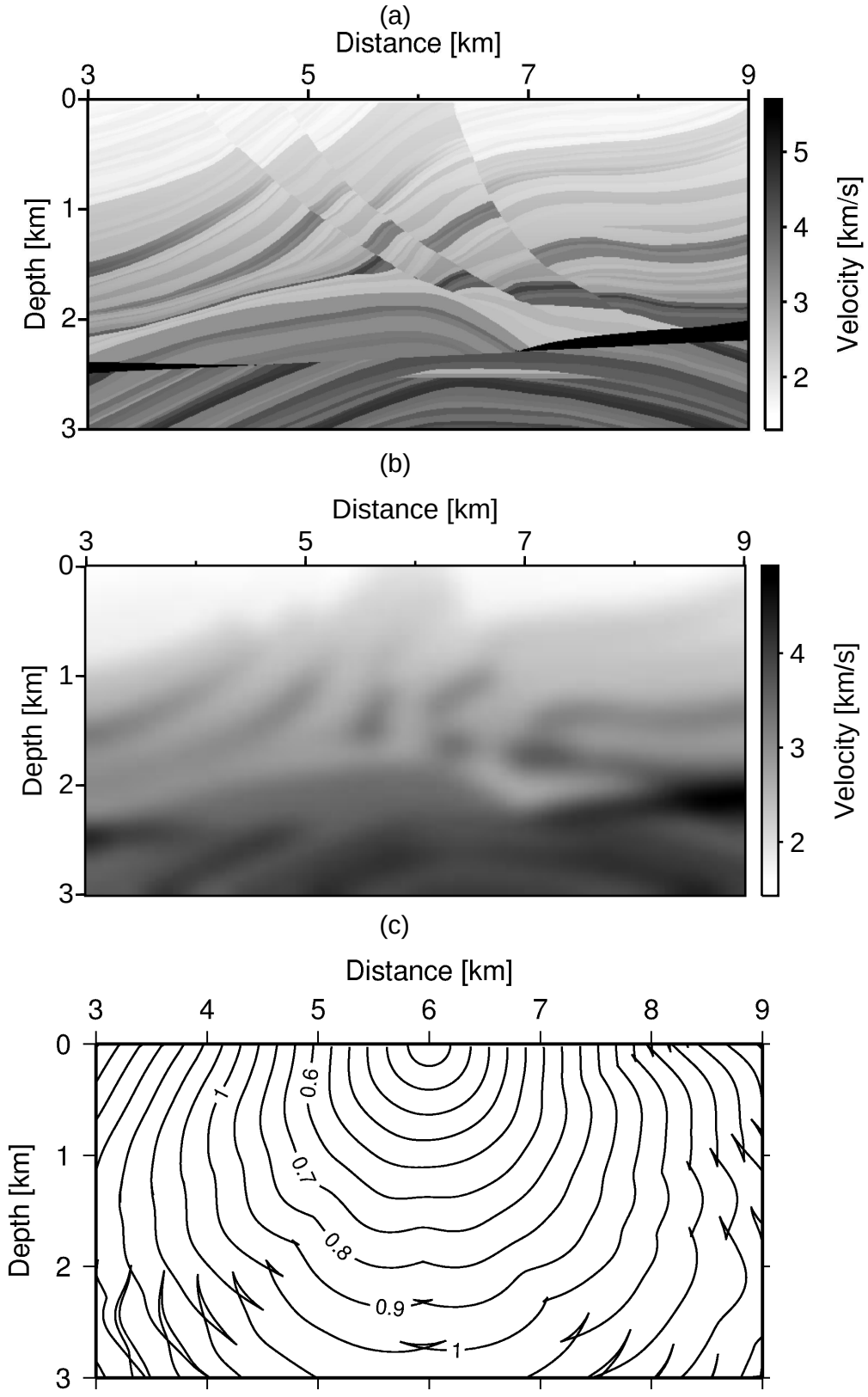


**Figure 4:** Marmousi model: (a) Unsmoothed velocity distribution. (b) Smoothed velocity distribution. (c) Isochrones plotted by using the reference traveltimes computed in the smoothed model. Contour interval is 0.1 s.

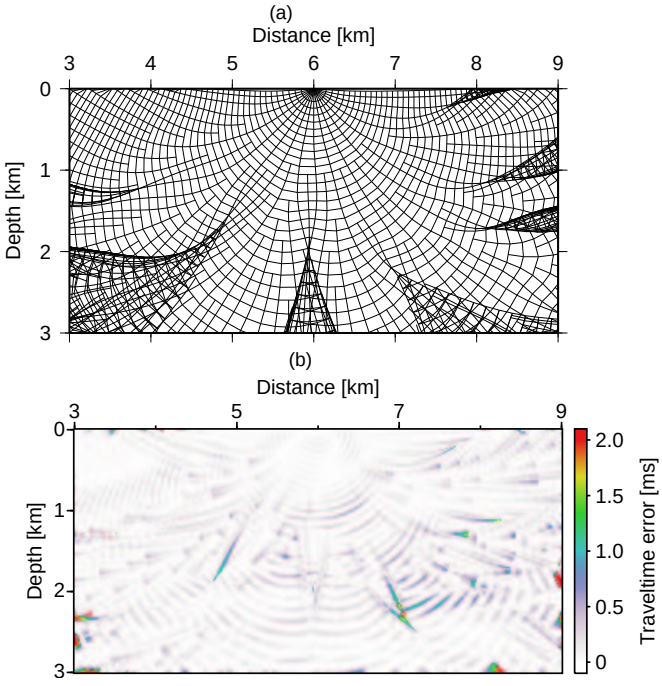


**Figure 5:** Second numerical example (see input parameters in Table 1). (a) Distribution of cells. Note that the rays are inserted by tracing from the source, but in this picture only the ray segments which bound cells are drawn. (b) Spatial distribution of the traveltime errors.

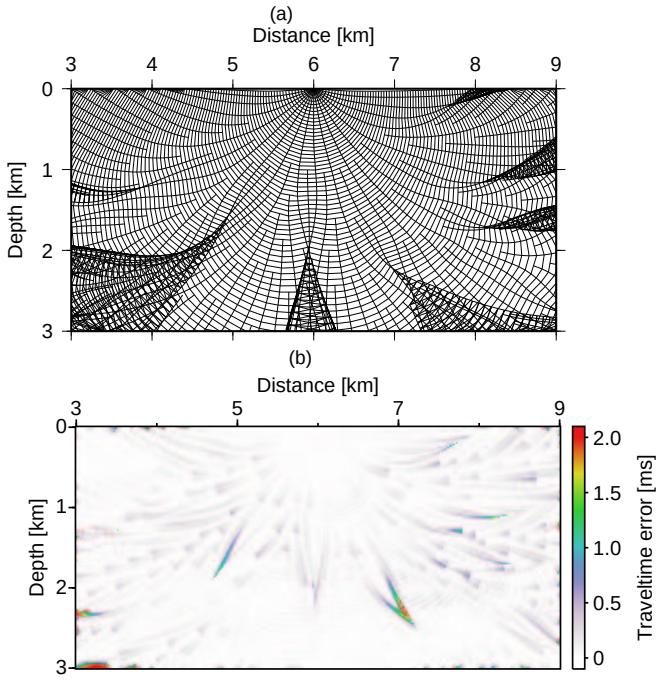


**Figure 6:** Third numerical example (see input parameters in Table 1). (a) Distribution of cells. (b) Spatial distribution of the traveltime errors.

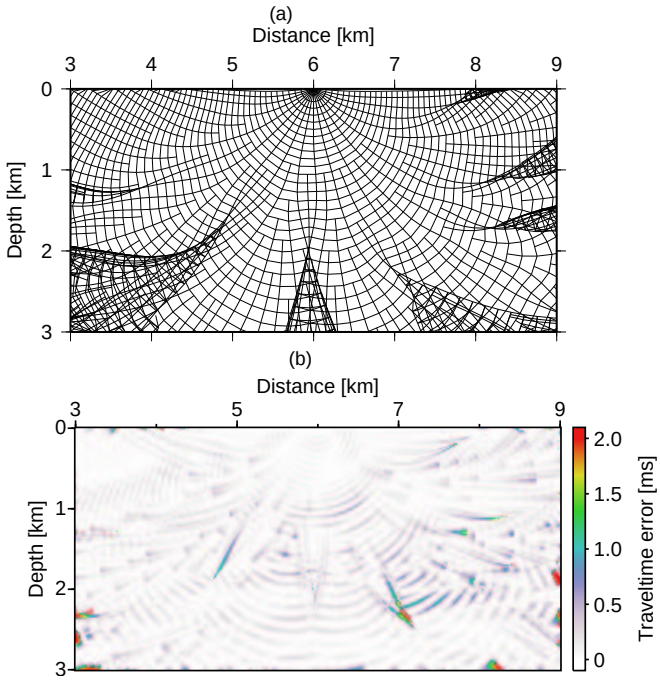


**Figure 7:** Fourth numerical example (see input parameters in Table 1). (a) Distribution of cells. (b) Spatial distribution of the traveltime errors.

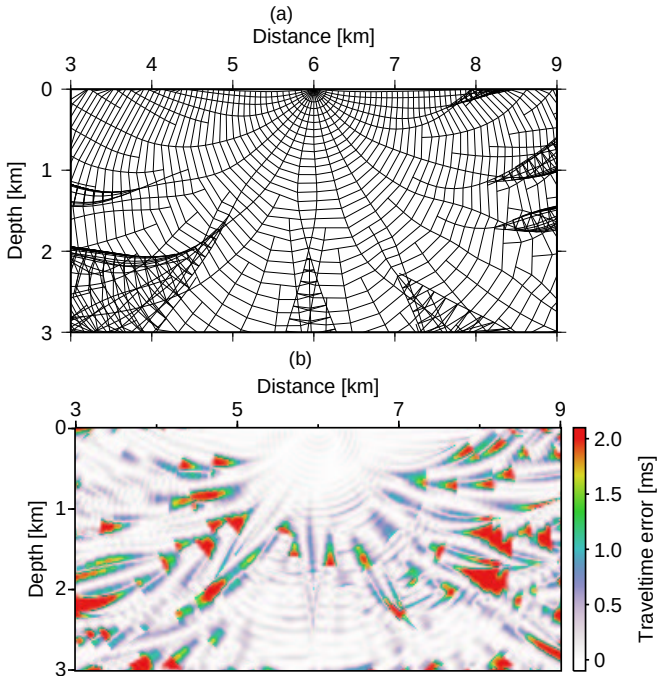


**Figure 8:** Fifth numerical example (see input parameters in Table 1). (a) Distribution of cells. (b) Spatial distribution of the traveltime errors.

by kinematic ray tracing. The insertion of new rays by tracing them from the source and the estimation of traveltimes by considering the wavefront curvature permit the use of large cells. The estimation of traveltimes in large cells requires less computational time than the estimation in smaller cells.

The accuracy and computational speed of the WRT technique is based on an optimal ray and wavefront density. The wavefront density is controlled by the time step of wavefronts. The ray density is controlled by three criteria for insertion of new rays. The node-distance insertion criterion minimizes errors caused by small-scale velocity anomalies. The time-difference insertion criterion reduces errors connected with the estimation of traveltimes at gridpoints. The crossing-ray insertion criterion reduces errors in caustic regions.

We have shown that the proposed WRT technique provides an efficient method for the computation of accurate traveltimes. In future work the method will be extended to three dimensions, where computational efficiency is even more important.

## ACKNOWLEDGMENTS

This work was partly supported by the sponsors of the *Wave Inversion Technology (WIT) Consortium*, Karlsruhe, Germany. We thank to Professor Boris Kashtan, Dr. Ekkehart Tessmer, Claudia Vanelle, Dr. Tim Bergmann, Tina Kaschwich, and Manfred Menyoli for valuable comments on the manuscript.

## REFERENCES

Åstebøl, K. (1994). Easy-to-use modelling – 3D ray field propagation in open ray models. In *Extended Abstracts*, page G015.

Bulant, P. (1999). Two-point ray tracing and controlled initial-value ray tracing in 3-D heterogeneous block structures. *J. Seis. Expl.*, 8:57–75.

Bulant, P. and Klimeš, L. (1999). Interpolation of ray theory traveltimes within ray cells. *Geophys. J. Int.*, 139:273–282.

Červený, V. (1985). The application of ray tracing to the numerical modeling of seismic wavefield in complex structure. In Dohr, G., editor, *Seismic Shear Waves*, volume Handbook of Geophys. Expl.,15A, chapter I, pages 1–124. Geophysical Press, London.

Ettrich, N. and Gajewski, D. (1996). Wavefront construction in smooth media for pre-stack depth migration. *Pageoph*, 148:481–502.

Geoltrain, S. and Brac, J. (1993). Can we image complex structures with first-arrival traveltime? *Geophysics*, 58:564–575.

Lambaré, G., Lucio, P., and Hanyga, A. (1996). Two-dimensional multivalued traveltime and amplitude maps by uniform sampling of a ray field. *Geophys. J. Int.*, 125:584–598.

Lambaré, G., Virieux, J., Madariaga, R., and Jin, S. (1992). Iterative asymptotic inversion in the acoustic approximation. *Geophysics*, 57:1138–1154.

Lucio, P., Lambaré, G., and Hanyga, A. (1996). 3D multivalued travel time and amplitude maps. *Pageoph*, 148:449–479.

Moser, T. and Pajchel, J. (1997). Recursive seismic ray modelling: applications in inversion and VSP. *Geophys. Prosp.*, 45:885–908.

Operto, S., Xu, S., and Lambaré, G. (2000). Can we quantitatively image complex structures with rays? *Geophysics*, 65:1223–1238.

Sun, Y. (1992). Computation of 2D multiple arrival travel time fields by an interpolative shooting method. In *Expanded Abstracts*, pages 1320–1323. Soc. Expl. Geophys.

Vanelle, C. and Gajewski, D. (2001). Second-order interpolation of traveltimes. *Geophys. Prosp. (in press)*.

Versteeg, R. and Grau, G. (1990). Practical aspects of seismic data inversion, the Marmousi experience. In *Proc. 1990 EAEG Workshop*, pages 1–194, Copenhaga. Eur. Assoc. Expl Geophys.

Vinje, V. (1997). A new interpolation criterion for controlling accuracy in wavefront construction. In *Expanded Abstracts*, pages 1723–1726. Soc. Expl. Geophys.

Vinje, V., Iversen, E., Åstebøl, K., and Gjøystdal, H. (1996a). Estimation of multivalued arrivals in 3D models using wavefront construction–Part I. *Geophys. Prosp.*, 44:819–842.

Vinje, V., Iversen, E., Åstebøl, K., and Gjøystdal, H. (1996b). Part II: Tracing and interpolation. *Geophys. Prosp.*, 44:843–858.

Vinje, V., Iversen, E., and Gjøystdal, H. (1993). Traveltime and amplitude estimation using wavefront construction. *Geophysics*, 58:1157–1166.